NANO LETTERS

2007
Vol. 7, No. 12
3709−3715

Fullerene Coalescence into Metallic Heterostructures in Boron Nitride Nanotubes: A Molecular Dynamics Study

Xiaoyan Li,[†] Wei Yang,*[,‡,†] and Bin Liu[†]

Department of Engineering Mechanics, Tsinghua University, Beijing 100084, People's Republic of China, and University Office, Zhejiang University, Hangzhou 310058, People's Republic of China

Received August 14, 2007; Revised Manuscript Received October 22, 2007

ABSTRACT

We report the full molecular dynamics simulations for fusing the encapsulated fullerene linear chain into a single-walled carbon nanotube when the boron nitride nanopeapods undergo thermal annealing at high temperature. Such supramolecular coalescence inside a one-dimensional confining environment, involving fullerene polymerization and surface reconstruction, is driven by surface and strain energy minimization. The evolution of vacancies and isomerization of carbon rings play the dominant role in the structural transformation. The internal pressure and temperature are crucial for the merging of fullerene molecules and the formation of corrugated carbon nanotube cores. Within the ab initio framework, we investigate the electronic, transport, and magnetic properties of heterostructures after phase transformation. The results indicate that the new phase is metallic due to a core of corrugated carbon nanotube, which provides an electron transport channel. Further analyses of energy bands and spin densities reveal the possibility of flat-band ferromagnetism in the heterostructures.

Physical mergence of fullerenes and carbon nanotubes (CNTs) has triggered a boom of both theoretical and experimental researches. Various novel hybrid carbon structures, such as nanopeapods and nanonuds, have been synthesized in different physicochemical methods.[1−4] In contrast to single-walled carbon nanotubes (SWCNTs) or fullerene alone, these hybrid structures possess advantageous electronic and transport properties.[4−7] Especially, nanopeapods are regarded as promising candidates for nanometer-sized containers,[3] quantum storage,[8−10] and possibly high-temperature superconductors.[7] The microscopic formation mechanism[11] of nanopeapods is investigated via molecular dynamics (MD) simulations. For nanopeapods with the lanthanide metallofullerene, the defect-mediated atomic migration[12] is demonstrated by the in situ transmission electron microscopy observations. Under electron irradiation or thermal annealing,[3−5,13] a chain of fullerene molecules inside SWCNTs coalesce into a small-diameter CNT. On the basis of theoretical calculations, such structural transformation strongly affects the electron conductance of nanopeapods.[14] Recently, the boron nitride nanotube peapods (BNNTPs) packed with C_{60} molecules were reported.[15] The temperature-induced fusing of C_{60} molecules occurs under concentrated electron beam irradiation, resulting in a CNT core sheathed by an insulating boron nitride nanotube (BNNT).[15] Meanwhile, it was predicted this coaxial nanostructure might lead to unusual conductivity.[16] In this letter, we perform MD simulations for coalescence of fullerene molecules inside double-walled BNNTs annealed at high temperature. Driven by surface and strain energy minimization, the merging process is a manifestation of fullerene polymerization and surface reconstruction that involves both breakage and formation of covalent bonds. Using the quantum mechanics calculations, we report the band structures and $I-V$ characteristics of BNNTPs before and after structural transformation. The results indicate a structural transformation from a modest gap semiconductor into a metallic conductor. On the basis of the analyses of spin densities, we show that the heterostructured nanotubes possibly possess the flat-band ferromagnetism.

To obtain the ordered phases of fullerene encapsulated in double-walled nanotubes, we carried out atomistic simulations proposed by Troche et al.[17] For C_{60} molecules inside (10,10) at (15,15) and (17,0) at (25,0) BNNTs, the mean center-to-center intermolecular distances are 0.89 ± 0.02 and 0.88 ± 0.02 nm, respectively, which are in good agreement with the experimental observation.[16] Table 1 presents data

* Corresponding author. E-mail: yangw@zju.edu.cn; yw-dem@tsinghua.edu.cn.
[†] Tsinghua University.
[‡] Zhejiang University.

10.1021/nl0720410 CCC: $37.00
Published on Web 11/14/2007

Table 1. Mean Intermolecular Distances for Different Fullerene Molecules Encapsulated Inside Double-Walled Nanotubes

fullerene (symmetry)	external nanotubes	inner radius of nanotubes (nm)	intermolecular spacing (nm)
C_{60} (I_h)	(10,10) at (15,15) BNNTs	0.692	0.89 ± 0.02
C_{60} (I_h)	(17,0) at (25,0) BNNTs	0.680	0.88 ± 0.02
C_{60} (I_h)	(10,10) at (15,15) CNTs	0.678	0.98 ± 0.02
C_{60} (I_h)	(10,10) at (15,15) SiCNTs	0.711	0.95 ± 0.03
C_{70} (D_{5h})	(11,11) at (16,16) BNNTs	0.761	1.04 ± 0.04
C_{72} (D_{6d})	(11,11) at (16,16) BNNTs	0.761	1.05 ± 0.04
C_{74} (D_{3h})	(11,11) at (16,16) BNNTs	0.761	1.05 ± 0.04
C_{76} (D_2)	(11,11) at (16,16) BNNTs	0.761	1.07 ± 0.04
C_{78} (C_{2v})	(11,11) at (16,16) BNNTs	0.761	1.06 ± 0.02
C_{80} (I_h)	(11,11) at (16,16) BNNTs	0.761	1.08 ± 0.02

Table 2. Parameters of Lennard-Jones Potential for Different Interatomic Interaction[21,22]

atom type	distance (nm)	energy ($\times 10^{-3}$eV)
C−C	0.340	3.732
B−B	0.364	7.811
N−N	0.326	2.994
Si−Si	0.383	17.444
C−B	0.352	5.399
C−N	0.333	3.343
C−Si	0.361	8.068
B−N	0.345	4.836

for fullerene arrangements in different double-walled nanotubes. On the basis of the linear fullerene chain with a constant spacing in Table 1, we construct the equilibrium configuration consisting of double-walled nanotubes and 20 complete fullerenes. MD simulations are carried out for all nanopeapod configurations by using empirical potentials. During MD simulations, the bonding interactions of boron−nitride and silicon−carbon are modeled with many-body Tersoff-like potentials,[18,19] and carbon−carbon bonding interaction is characterized by reactive empirical bond order potential, which allows for covalent bond forming and breaking, with associated changes in atomic hybridization.[20] The van der Waals (vdWs) force is described by using Lennard-Jones (LJ) 6−12 potential with a cutoff distance of 1.5 nm. The corresponding parameters[21,22] for LJ potential are listed in Table 2. To improve the computational efficiency, a multiple time step algorithm[23,24] with the shorter and longer time steps of 0.5 and 1.5 fs, respectively, is used. The periodic boundary conditions are imposed in the axial direction of double-walled nanotubes. Before MD simulations, we perform geometrical optimizations to obtain the energy minimization of initial configurations via conjugate gradient method. Throughout MD simulations, a Nose−Hoover thermostat[24−26] is adopted to control and adjust the temperature of the simulated system. To mimic a Gatan heating at high temperature under electron irradiation,[27] the temperature is gradually increased from 300 K by a time step of 0.0085 K. After 100 ps, the temperature of the system reaches 2000 K and then keeps constant for 200 ps. During the last 100 ps, the temperature is slowly cooled from 2000 to 300 K through the annealing relaxation technology.[27] The above thermodynamics procedure not only actualizes the high-temperature circumstance similar to experimental situations under electron beam irradiation, but also accelerates the structural changes and the switching of covalent bonds. The latter would further promote both the coalescence and the formation of interconnections between neighboring fullerene molecules.

The electronic properties of the structures before and after transformation have been calculated in ab initio density functional theory (DFT), as implemented in the CPMD package.[28] The exchange-correlation energy is evaluated using the local density approximation. The interaction between the valence electrons and ionic cores is described through fully nonlocal norm-conserving Troullier−Martins pseudopotentials[29] in the Kleinman−Bylander[30] separable form. The wave-functions are expanded by the plane-wave basis set with a kinetic energy cutoff of 70 Ry. The supercell model is used to perform the structural relaxations. In the present scheme, we impose a commensurability condition between the one-dimensional periodicity of atomic arrangements in the nanotube and that of the C_{60} chain. Consequently, the lattice parameter of the unit cell becomes 1.046 nm along the nanotube direction, and other sizes of the unit cell are chosen to be sufficiently large to avoid any spurious image effects on the calculated total energy. To study the magnetism in the heterostructures, we have performed the electronic structure calculations based on the local spin density approximate (LSDA) with the Ceperley−Adler exchange-correlation functional formalism.[31,32]

Figure 1 shows a sequence of snapshots during MD simulations. Initially, the adjacent fullerenes are connected by single bonds with the hybridization from sp^2 to sp^3.[33] Further dimerization of fullerenes leads to producing dimers and then trimers via the cycloaddition reaction,[33] which strengthens the interfullerene binding and partly relieves structural strain. As the temperature is increased, the fullerenes are gradually polymerized by the formation of bonding bridges and four-membered rings. Subsequently, the fullerenes tend to coalesce in a more compact configuration, forming a pearl necklacelike structure with the local negative curvature.[14] Sustained under a constant temperature, the surface reconstruction occurs by switching of covalent bonds, such as bond breakage and bond formation. Through the thermal annealing, the encapsulated structure evolves toward a small-diameter corrugated nanotube for the sake of reduction in surface energy. Such reconstruction process

Table 3. Distributions of Carbon Rings on the Cores Encapsulated in Different External Nanotubes

external nanotubes	numbers of carbon rings				ratio of hexagons to nonhexagons
	pentagon	hexagon	heptagon	octagon	
(10,10) at (15,15) BNNTs	39	367	60	19	3.11
(17,0) at (25,0) BNNTs	43	346	56	13	3.08
(10,10) at (15,15) CNTs	34	284	49	36	2.39
(10,10) at (15,15) SiCNTs	60	321	50	23	2.41

involves defect generation and presence of reactive surface sites, such as vacancies, interstitials, dangling bonds, and Stone−Wales defects. The nucleation and the movement of defects dictate the optimization of the atomic structure. Reisomerization of the 5/7 ring to two hexagons is commonly observed at temperatures below 2000 K, indicating the reduction in the local structural strain energy. Interestingly, some octagonal or larger carbon rings form due to the lack of π-conjunctional stabilization.[34] Several cyclic structures vanish and change into the 5/7 ring combinations under the thermal fluctuation. Eventually, the resulting nanotube consists of pentagons, hexagons, heptagons, and octagons. The local region of the nanotube core exhibits the feature of Haeckelite structure,[35,36] which is a metastable sp^2-like carbon network. Table 3 summarizes the numbers of several carbon rings in the nanotube cores confined within different external nanotubes. The cores in the armchair and zigzag BNNTs have a higher ratio of hexagons to nonhexagons, relative to those in C- and SiC-NTs. This implies that the fullerene coalescence is favorable in the BNNTs. The armchair BNNTs would induce slightly more defects on the core than those in the zigzag tubes. However, there are less pentagon-heptagon pairs on the cores in armchair BNNTs than those in zigzag ones. This might be associated with the chirality of external nanotubes, as well as the commensurance between the outer sheath and inner core.

To further investigate the factors affecting fullerene coalescence, we carry out MD simulations for all of nanopeapod cases listed in Table 1. For chains of C_{60} molecules encapsulated inside double-walled C-, SiC-, and BN-nanotubes, Figure 2 depicts their final configurations obtained from MD simulations. The atoms are painted in term of their potential energies in Figure 2a with the color bar set in Figure 1, while atoms are identified by their initial positions on the C_{60} molecules in Figure 2b. The nanotube core confined in double-walled BNNTs has better tubular structure than those in C- and SiC-nanotubes. Obviously, the nanotube core in CNTs has several distinct defects featured with few carbon rings connecting the overall structure, while the core inside SiCNTs is reminiscent of a pearl necklacelike structure with local negative curvature. During the polymerization and reconstruction of fullerene molecules, atomic migration is occurred inside nanotube peapod, as illustrated in Figure 2b. In particular, the displacements of some atoms exceed the diameter of a single C_{60} molecule. Such atomic transfer is mediated by propagation of defects, which demonstrates the solid-state diffusion of individual atoms. By tracking the dynamic behavior of certain atoms, we observe that the motion of vacancies and isomerization of carbon rings promote the atomic migration through the bonding hybridization.

The above differences of evolution inside three nanopeapods are closely associated with the pressure provided by external nanotubes. The pressure that the polymerized fullerenes are subjected to is originated from vdWs interaction between the external nanotubes and the fullerene molecules. Because the fullerenes confined within heterogeneous nanotubes bear different internal pressure, the C_{60}−C_{60} intermolecular distances for three nanopeapods exhibit slight differences in Table 1. During MD simulations, we estimate the average values of internal pressure inside three nanopeapods by calculating the radial forces on the fullerene chain. The zigzag and armchair BNNTPs are found to process the higher internal pressure of 37.8 and 32.9 GPa, while the pressures inside C- and SiC-nanopeapods are 16.6 and 22.8 GPa, respectively. It is evident that the high-pressure inside the nanopeapods is energetically favorable for the polymerization of fullerenes. Apart from the internal pressure, the temperature is crucial for the fullerene coalescence. The thermal process ensures a high mobility of atoms and hence rapid healing of defects. Under the high-temperature conditions, the nanotube core forming within the one-dimensional confinement would shrink by mending the surface defects through atomic rearrangements, leading to surface reconstruction and topological changes.

For the structural transformation from chainlike to tubular configurations, we analyze the possibility and the stability of fullerene coalescence. Figure 3 displays the relations between the energy variation and the intermolecular distance for different fullerene chains in double-walled BNNTs. From the energy viewpoint, the conversion from fullerene chain to tubule is available when the fullerenes overcome the energy barrier of supramolecular merging under the thermal fluctuation. Because of the closed bonding structure with a certain extreme curvature, fullerenes have a higher cohesive energy relative to the graphitic nanotubes. Therefore, the minimization of strain energy provides a strong driving force for the structural transformation of the fullerene chain. Combined with the existence of thermodynamic driving force, the coalescence of fullerene molecules and the formation of nanotube core are kinetically favored. As shown in Figure 3, the energy variations of structural transformation decrease with an increase of the intermolecular spacing. This is attributed to the opposite trends between the increase of distributing distance of fullerenes and the occurrence of polymerization. Actually, the equilibrium distance of two adjacent fullerenes distributed in double-walled nanotubes is related to the structural geometries of the fullerene, such

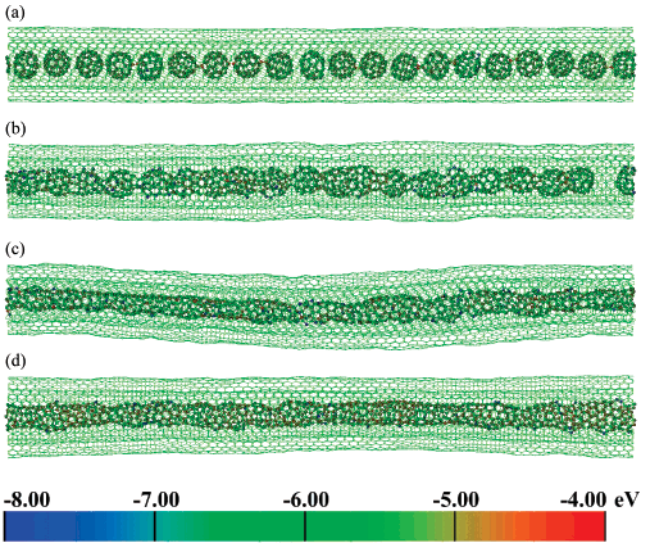

Figure 1. Sequential images showing the coalescence of fullerene molecules inside double-walled BNNTs: (a) 16, (b) 56, (c) 200, and (d) 360 ps.

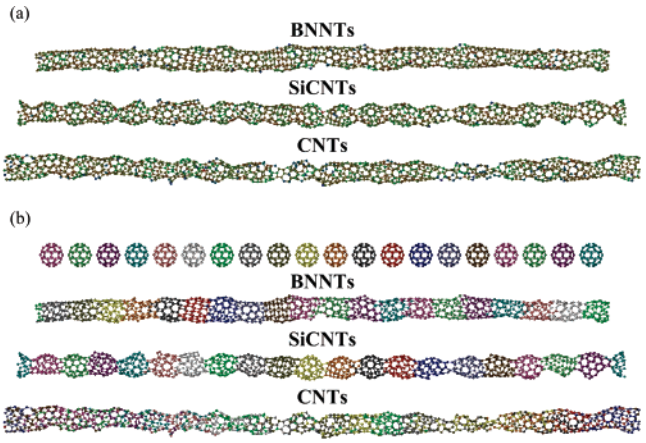

Figure 2. Final configurations of inner CNT core within double-walled BN-, SiC-, and C-nanotubes: (a) identification by potential energy of atoms (see color bar in Figure 1), (b) identification by initial position of atoms.

as number, symmetry, and arrangement of pentagonal and hexagonal rings.[17,37] The absolute value of energy variation in the zigzag BNNTs is larger than that in the armchair ones, implying an argument that the fullerene merging is preferential for BNNTs with the zigzag chirality.

Inspired by the prediction about unusual conductivity of BNNTPs,[15] we explore the electronic properties of phases before and after the structural transformation. Figure 4a−c shows the periodic structures of (10,10) BNNT, perfect nanopeapod, and new phase after temperature-induced transformation, respectively. The configurations shown in Figure 4b,c are chosen from the results of classical MD simulation and then are obtained through the structural relaxation and wave function optimization in the CPMD package.[28] The band structures and the density of states for three structures are shown in Figure 4d. The Fermi level is identified by a dotted line and is taken as the energy of reference. One band crosses the Fermi level in structure after transformation, implicating that the transformed phase has

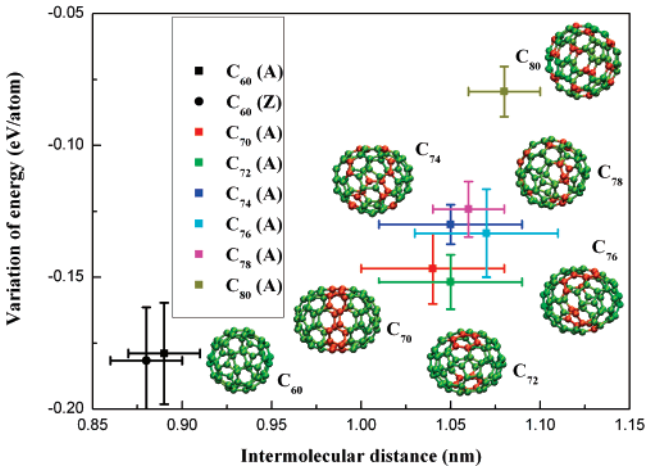

Figure 3. Relations between energy variation and intermolecular distance for different fullerene chains encapsulated in double-walled BNNTs. Here the label A represents armchair, and Z means zigzag. Atoms are colored according to potential energy (see color bar in Figure 1).

metallic electronic structure different from the perfect nanopeapod before transformation and the single-walled BNNT. The present calculations indicate that accommodating C_{60} molecule into a broad-gap semiconducting BNNT has the effect of narrowing the band gap at the Fermi level. It is noteworthy that the fullerenes coalescence leads to lower dispersion of bands in the structure after transformation relative to a perfect nanopeapod. This behavior is attributed to the loss of symmetry due to the structural transition.

To confirm the electronic and transport properties of BNNTPs, we calculate the quantum conductances of structures before and after transformation using a combined nonequilibrium Green's function and DFT-based formalism.[38−40] Two representative electrodes are employed: one is (10,10) CNT with a length of 0.879 nm, and another is (100)-oriented Ag slab with a dimension of $0.614 \times 1.432 \times 1.432$ nm^3. The equilibrium binding distance between the electrodes and the examined samples is obtained by the full ab initio optimization for side-contact geometry,[41] which assures a reasonably strongly coupled contact. The distance between CNT and samples is about 0.145 nm, while the distance between solid Ag and samples is 0.218 nm. Figure 5 depicts the current versus voltage ($I-V$) characteristics of structures before and after transformation for CNT and solid Ag electrodes. The $I-V$ characteristics of devices with CNT electrodes remain consistent, and the slight differences arise from the rather weak interactions between outer sheath and inner core. However, the devices with solid Ag electrodes display the distinct differences in the $I-V$ characteristics. This observation indicates that the inner core forming through structural transformation provides an electron transport channel, while the outer sheath acts as a broad band gap semiconductor. Therefore, the structural transformation involving fullerene coalescence is electronically a semiconductor−metal transition.

Recently, the ferromagnetisms in the all-carbon system with polymerized C_{60},[42] BN/C heterostructured nanosheets[43,44] and nanotubes[45] were discovered via experimental and

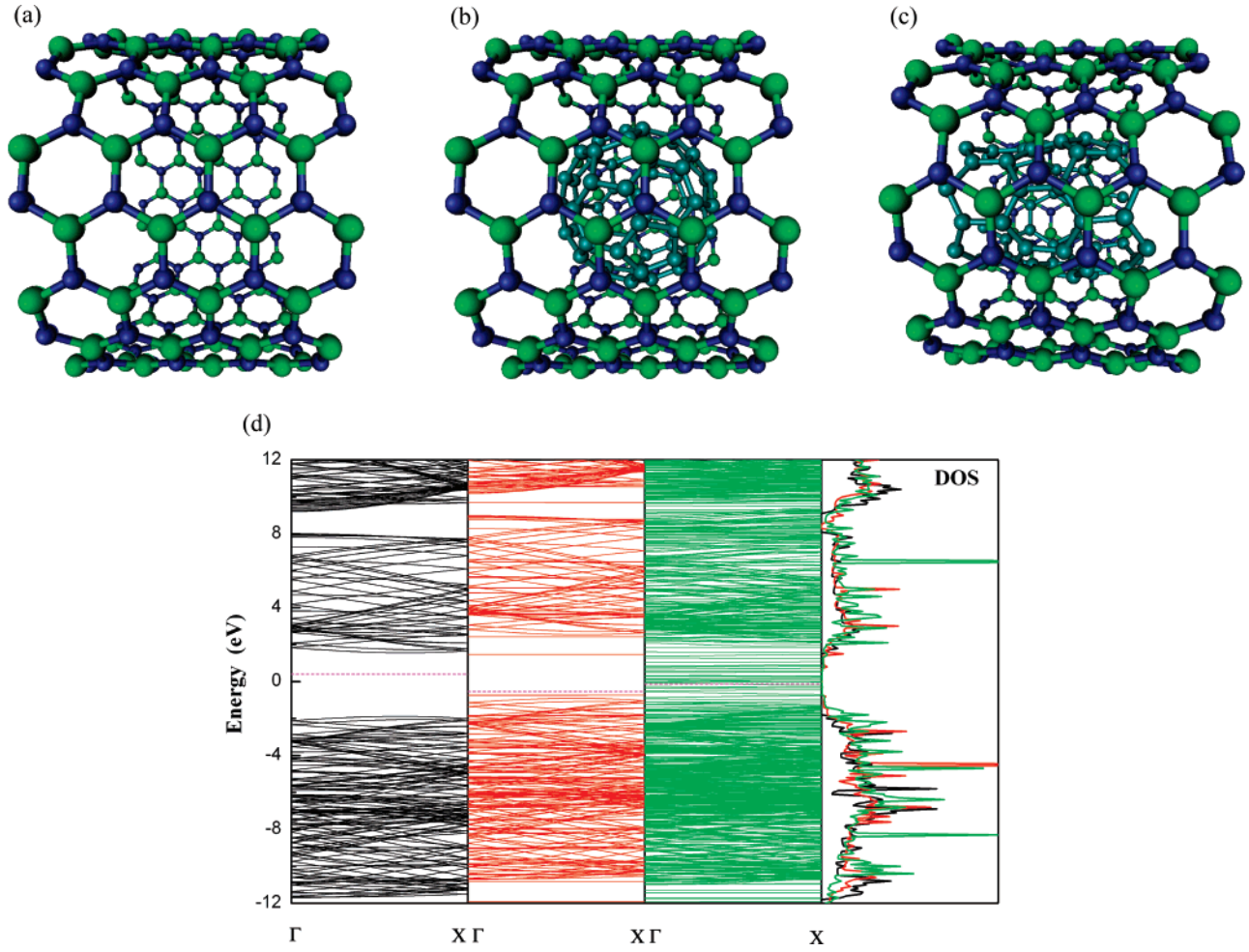

Figure 4. Band structures and electronic density of states for three periodic structures. Black, red, and green lines correspond to the results of (a) single (10,10) BNNT, (b) perfect BNNTP, and (c) new phase after structural transformation, respectively.

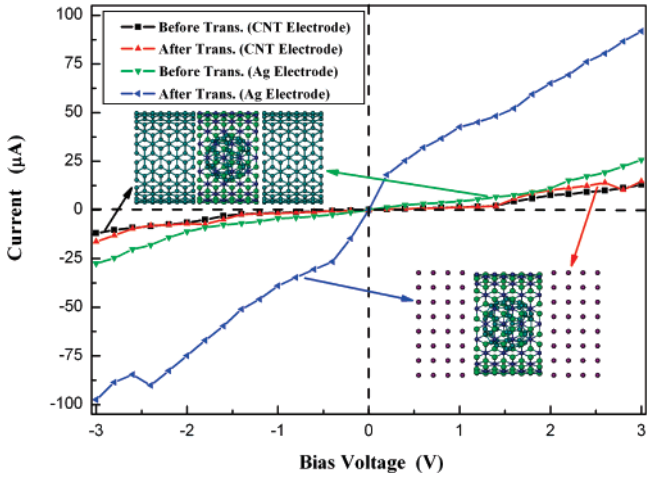

Figure 5. *I*−*V* characteristics of structures before and after transformation for CNT and solid Ag electrodes.

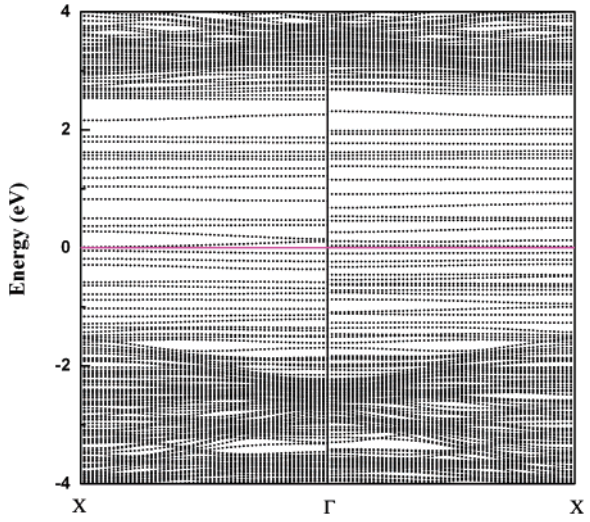

Figure 6. Energy bands of heterostructure after transformation for majority (left) and minority (right) spins with the Fermi level set to be 0 eV.

theoretical studies. To predict the probability of ferromagnetism in the heterostructure consisting of BNNT shells and corrugated CNT core, we perform the total-energy electronic-structure calculations based on LSDA. Figure 6 shows the calculated band structure of new phase for the majority and minority spins. One important feature is the occurrence of flat bands in the vicinity of Fermi level, whose dispersions are very small, only a few tenths of eV. These flat-band states are introduced by the structural transformation and are associated with the core configuration from polymerization of C_{60} molecules. Such flat-band states for majority and minority spins are analogous to those found in the ferro-

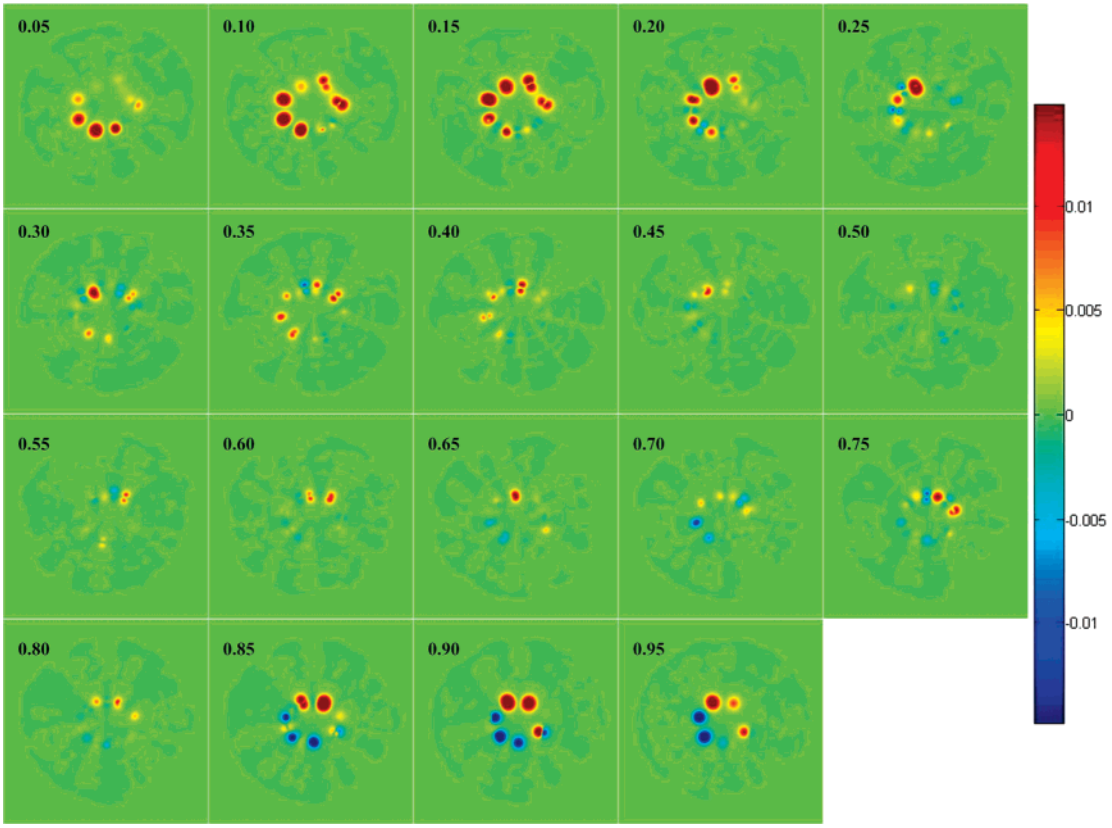

Figure 7. Contour distributions of the spin densities $[n_{\uparrow}(r) - n_{\downarrow}(r)]$ on the different cross section of heterostructure after transformation. The spin densities are in units of 1/bohr^3. The value in the upper left corner stands for the ratio of position of current cross section to size of superlattice cell.

magnetic BN/C nanosheets.[44] The contour distributions of the spin density $n_{\uparrow}(r) - n_{\downarrow}(r)$ on the different cross sections, where the up spin is the majority, are depicted in the Figure 7. On some cross sections, it is reflected that the magnetic ordering occurred in the nanotube core. Such magnetic ordering corresponds to the flat-band states from polymerized C_{60}. If one examines effects of carrier doping on the magnetic ordering in the heterostructure, it is possible that the ferromagnetic state is observed in the doped system.

In summary, we show a fascinating structural transformation, fullerene coalescence, inside double-walled BNNTs under thermal annealing via classical MD simulations. This transformation is driven by surface and strain energy minimization. The transformation involves fullerene polymerization and surface reconstruction, while the latter contains evolution of vacancies and isomerization of carbon rings. It is demonstrated that the internal pressure and surrounding temperature are two significant factors affecting fullerene coalescence. Using the quantum mechanics calculations, we predict that the heterostructure after transformation displays a metallic behavior because a CNT core encased within a semiconducting BNNT provides a channel for electron transport. By analyzing the spin densities of the heterostructure, we find that this heterostructure is a possible example of the flat-band ferromagnetism originated from polymerized C_{60}. Further exploitation for the local metallic transitions and special magnetic properties may have potential applications in nanoscale devices. It is envisioned that nanotubes with different chiralities can be welded by fusing fullerenes like soldering tins, thus indicating a blueprint to synthesis of nanoelectronic devices, such as nanotube heterojunctions[46] and quantum dots.[47]

Acknowledgment. This work was supported by grants from the National Natural Science Foundation of China (No. 10332020 and No. 10121202) and from the 973 Projects of China (No. 2004CB619304). The authors also thank the Chinese Academy of Meteorological Science for the supports of parallel computation on IBM1600 supercomputer.

References

(1) Smith, B. W.; Monthioux, M.; Luzzi, D. E. *Nature* **1998**, *396*, 323.
(2) Burteaux, B.; Calye, A.; Smith, B. W.; Monthioux, M.; Luzzi. D. E.; Fischer, J. E. *Chem. Phys. Lett.* **1999**, *310*, 21.
(3) Smith, B. W.; Luzzi, D. E. *Chem. Phys. Lett.* **2000**, *321*, 169.
(4) Nasibulin, A. G.; Pikhutsa, P. V.; Jiang, H.; Brown, D. P.; Krasheninnikov, A. V.; Anisimov, A. S.; Queipo, P.; Moisala, A.; Gonzalez, D.; Lientschnig, G.; Hassanien, A.; Shandakov, S. D.; Lolli, G.; Resasco, D. E.; Choi, M.; Tománek, D.; Kauppinen, E. I. *Nat. Nanotechnol.* **2007**, *2*, 156.
(5) Okada, S.; Saito, S.; Oshiyama, A. *Phys. Rev. Lett.* **2001**, *86*, 3835.
(6) Hornbaker, D. J.; Kahng, S. J.; Misra, S.; Smith, B. W.; Johnson, A. T.; Mele, E. J.; Luzzi, D. E.; Yazdani, A. *Science* **2002**, *295*, 828.
(7) Service, R. F. *Science* **2001**, *292*, 45.
(8) Kwon, Y.-K.; Tománek, D.; Iijima, S. *Phys. Rev. Lett.* **1999**, *82*, 1470.
(9) Suenaga, K.; Tencé, M.; Mory, C.; Colliex, C.; Kato, H.; Okazaki, T.; Shinohara, H.; Bandow, S.; Iijima, S. *Science* **2000**, *290*, 2280.
(10) Lee, J.; Kim, H.; Kahng, S. J.; Kim, G.; Son, Y. W.; Ihm, J.; Kato, H.; Wang, Z. W.; Okazaki, T.; Shinohara, H.; Kuk, Y. *Nature* **2002**, *415*, 1005.
(11) Berber, S.; Kwon, Y. K.; Tománek, D. *Phys. Rev. Lett.* **2002**, *88*, 185502.

(12) Urita, K.; Sato, Y.; Suenaga, K.; Gloter, A.; Hashimoto, A.; Ishida, M.; Shimada, T.; Shinohara, H.; Iijima, S. *Nano Lett.* **2004**, *4*, 2451.
(13) Sloan, J.; Dunin-Borkowski, R. E.; Hutchison, J. L.; Coleman, K. S.; Williams, V. C.; Claridge, J. B.; York, A. P. E.; Xu, C.; Bailey, S. R.; Brown, G.; Friedrichs, S.; Green, M. L. H. *Chem. Phys. Lett.* **2000**, *316*, 191.
(14) Hernández, E.; Meunier, V.; Smith, B. W.; Rurali, R.; Terrones, H.; Nardelli, M. B.; Terrones, M.; Luzzi, D. E.; Charlier, J. C. *Nano Lett.* **2003**, *3*, 1037.
(15) Mickelson, W.; Aloni, S.; Han, W.; Cumings, J.; Zettl, A. *Science* **2003**, *300*, 467.
(16) Zettl, A.; Cumings, J.; Han, W.; Mickelson, W. In *Structural and Electronic Properties of Molecular Nanostructures*; Kuzmany, H., Ed.; American Institute of Physics: New York, 2002; pp 140−144.
(17) Troche, K. S.; Coluci, V. R.; Braga, S. F.; Chinellato, D. D.; Sato, F.; Legoas, S. B.; Rurali, R.; Galvão, D. S. *Nano Lett.* **2005**, *5*, 349.
(18) Albe, K.; Möller, W. *Comp. Mater. Sci.* **1998**, *10*, 111.
(19) Tersoff, J. *Phys. Rev. B.* **1988**, *38*, 9902.
(20) Brenner, D. W.; Shenderova, O. A.; Harrison, J. A.; Stuart, S. J.; Ni, B.; Sinnott, S. B. *J. Phys.: Condens. Matter* **2002**, *14*, 783.
(21) Rappé, A. K.; Casewit, C. J.; Colwell, K. S.; Goddard, W. A., III; Skiff, W. M. *J. Am. Chem. Soc.* **1992**, *114*, 10024.
(22) Hummer, G.; Rasaiah, J. C.; Noworyta, J. P. *Nature* **2001**, *414*, 188.
(23) Tuckerman, M.; Berne, B. J.; Mantyna, G. J. *J. Chem. Phys.* **1992**, *97*, 1990.
(24) Li, X.; Yang, W.; Liu, B. *Phys. Rev. Lett.* **2007**, *98*, 205502.
(25) Nose, S. A. *J. Chem. Phys.* **1984**, *81*, 511.
(26) Hoover, W. G. *Phys. Rev. A.* **1985**, *31*, 1695.
(27) Terrones, M.; Terrones, H.; Banhart, F.; Charlier, J. C.; Ajayan, P. M. *Science* **2000**, *288*, 1226.
(28) CPMD package; Copyright IBM Corp 1990−2005, MPI für Festkörperforschung Stuttgart 1997−2001; http://www.cpmd.org (accessed February 24, 2006).
(29) Troullier, N.; Martins, J. L. *Phys. Rev. B.* **1991**, *43*, 1993.
(30) Kleinman, L.; Bylander, D. M. *Phys. Rev. Lett.* **1982**, *48*, 1425.
(31) Ceperley, D. M.; Alder, B. J. *Phys. Rev. Lett.* **1980**, *45*, 566.
(32) Perdew, J. P.; Zunger, A. *Phys. Rev. B.* **1981**, *23*, 5048.
(33) Berber, S.; Osawa, E.; Tománek, D. *Phys. Rev. B.* **2004**, *70*, 085417.
(34) Irle, S.; Zheng, G.; Elstner, M.; Morokuma, K. *Nano Lett.* **2003**, *3*, 1657.
(35) Terrones, H.; Terrones, M.; Hernández, E.; Grobert, N.; Charlier, J. C.; Ajayan, P. M. *Phys. Rev. Lett.* **2000**, *84*, 1716.
(36) Rocquefelte, X.; Rignanese, G. M.; Meunier, V.; Terrones, H.; Terrones, M.; Charlier, J. C. *Nano Lett.* **2004**, *4*, 805.
(37) Hirahara, K.; Bandow, S.; Suenaga, K.; Kato, H.; Okazaki, T.; Shinohara, H.; Iijima, S. *Phys. Rev. B.* **2001**, *64*, 115420.
(38) Jauho, A. P.; Wingreen, N. S.; Meir, Y. *Phys. Rev. B.* **1994**, *50*, 5528.
(39) Taylor, J.; Guo, H.; Wang, J. *Phys. Rev. B.* **2001**, *63*, 121104.
(40) Odbadrakh, K.; Pomorski, P.; Roland, C. *Phys. Rev. B.* **2006**, *73*, 233402.
(41) Shan, B.; Cho, K. *Phys. Rev. B.* **2004**, *70*, 233405.
(42) Makarova, T. L.; Sundqvist, B.; Höhne, R.; Esquinazis, P.; Kopelevich, Y.; Scharff, P.; Davydov, V. A.; Kashevarova, L. S.; Rakhmanina, A. V. *Nature* **2001**, *413*, 716.
(43) Okada, S.; Igami, M.; Nakada, K.; Oshiyama, A. *Phys. Rev. B.* **2000**, *62*, 9896.
(44) Okada, S.; Oshiyama, A. *Phys. Rev. Lett.* **2001**, *87*, 146803.
(45) Choi, J.; Kim, Y.; Chang, K. J.; Tománek, D. *Phys. Rev. B.* **2003**, *67*, 125421.
(46) Chico, L.; Crespi, V. H.; Benedict, L. X.; Louir, S. G.; Cohen, M. L. *Phys. Rev. Lett.* **1996**, *76*, 971.
(47) Chico, L.; Sancho, M. P. L.; Muñoz, M. C. *Phys. Rev. Lett.* **1998**, *81*, 1278.

NL0720410